Novel Ω-Shaped Core–Shell Photodetector with High Ultraviolet Selectivity and Enhanced Responsivity

Mingxiang Hu, Feng Teng, Hongyu Chen, Mingming Jiang, Yuzhu Gu, Hongliang Lu, Linfeng Hu, and Xiaosheng Fang**

The design of nanostructure plays an important role in performance enhancement of low-dimensional optoelectronic devices. Herein, a novel photodetector (PD) based on electrospun SnO_2 nanofibers with Ω-shaped ZnO shell (SnO_2@ZnO) is fabricated. With 87.4% transmittance at 550 nm, SnO_2@ZnO PD exhibits a high photo-to-dark current ratio up to 10^4 at around 280 nm. Owing to the additional Ω-shaped ZnO shell, SnO_2@ZnO PD possesses a responsivity of nearly 100 A W^{-1} under 5 V bias and the illumination of 250 nm light, which is 30-time enhancement of pristine SnO_2 PD. The enhancement is mainly attributed to type-II energy band structure. Furthermore, by changing the direction of incident light, SnO_2@ZnO PD has a high UV selectivity with an UV–vis rejection ratio ($R_{250\ nm}/R_{400\ nm}$) as much as 2.0×10^3 at 5 V bias under back illumination, which is fourfold higher than that under face illumination. The UV selectivity improvement may be attributed to light confinement in the Ω-shaped structure. With both theoretical simulations and experimental comparisons, it is demonstrated that the unique compact Ω-shaped nanostructure does contribute to photon trapping and gaining process, especially in back-illumination configuration. The approach can be easily extended to other materials, preparing novel building blocks for optoelectronic devices.

1. Introduction

Last 10 years have witnessed the rise of low-dimensional structured materials, including 0D, 1D, 2D materials, and their combinations.[1] For example, owing to the high surface-to-volume ratio and comparable scale with Debye length,[2] quasi-1D (Q1D) structured materials can be used in a variety of fields, such as light-emitting diode,[3] energy harvesters,[4] solar cells,[5] photodetectors,[6] etc. Among them, ultraviolet photodetectors (UV PDs) are of particular interest,[7] because the properties of Q1D structures (e.g. large responsivity and high photoconductive gain) enable their potential applications in fire monitoring, environmental sensors, and underwater communications.[8] Thus, a good choice of UV sensitive materials with a proper structure would be helpful in improvement of PD performance.[9]

Traditionally, metal oxides with wide bandgaps are good candidates for UV detection, such as ZnO,[10] SnO_2,[11] Ga_2O_3,[12] etc. PDs based on such materials exhibit superior electrical and optical properties. It is reported that single-crystal SnO_2 nanowire-based PDs possess ultrahigh external quantum efficiency and excellent UV selectivity.[13] Besides material selection, researchers have also found that some geometric nanostructures would benefit the PD performance. Zhai and co-workers reported a PD based on a kinked single-crystal SnO_2 nanowire, showing ultrahigh responsivity and improved photoresponse time comparing to the straight counterpart.[14] And compared to WO_3 nanofibers (NFs), polycrystalline WO_3 nanobelts synthesized by electrospinning resulted in an enhanced photo-to-dark current ratio up to 1000.[15] However, single material usually has its limitations, such as low sensitivity and responsivity, and many efforts are made to combine two materials into one structure in order to bridge the gap.[16] Among them, core–shell structure distinguishes itself due to its large clear interface of junction and controllable preparation.[17] For example, Chaaya et al. reported a performance-enhanced PD based on polyacrylonitrile/ZnO core–shell nanostructures by the atomic layer deposition (ALD) technique combined with

M. X. Hu, Dr. F. Teng, Prof. L. F. Hu, Prof. X. S. Fang
Department of Materials Science
Fudan University
Shanghai 200433, P. R. China
E-mail: linfenghu@fudan.edu.cn; xshfang@fudan.edu.cn
Dr. H. Y. Chen
Department of Physics
Harbin Institute of Technology
Harbin 150001, P. R. China
The ORCID identification number(s) for the author(s) of this article can be found under https://doi.org/10.1002/adfm.201704477.

DOI: 10.1002/adfm.201704477

Prof. M. M. Jiang
State Key Laboratory of Luminescence and Applications
Changchun Institute of Optics
Fine Mechanics and Physics
Chinese Academy of Sciences
Changchun 130033, P. R. China
Y. Z. Gu, Prof. H. L. Lu
State Key Laboratory of ASIC and System
Shanghai Institute of Intelligent Electronics and Systems
School of Microelectronics
Fudan University
Shanghai 200433, P. R. China

the electrospinning techniques.[18] There are also many other reported PDs based on the core–shell structure, such as SnO_2@TiO_2,[19] TiO_2@ZnO,[20] ZnO@NiO,[21] ZnO@CdS,[22] etc. Such a structure is beneficial for separating photogenerated carriers. In order to make full use of incoming light, shell materials usually possess wider bandgap so that the core material could convert the unabsorbed photons with lower energy into photocurrent. This, however, hinders the performance of core materials in UV detection and lowers the UV selectivity, since the cutoff wavelength of core is longer than that of shell. Therefore, a new structure for high-selective UV detection is needed.

Herein, combining electrospinning with ALD technique, we designed Ω-shaped core–shell nanostructure so as to enhance the light utilization of core. We coated the electrospun SnO_2 NF arrays with a ZnO layer in Ω shape via ALD method (denoted as SnO_2@ZnO), except for the contact area between SnO_2 and the substrate. The measured photo-to-dark current ratio at 280 nm is more than four orders of magnitude. With this peculiar structure, the responsivity of SnO_2@ZnO PD in UV region is improved by 30 times compared to that of bare SnO_2 NF-based PD. The direction of light also has influence on the performance of SnO_2@ZnO PD. Compared with the performance under face illumination, SnO_2@ZnO PD shows a higher UV selectivity with a high UV–vis rejection ratio ($R_{250\ nm}/R_{400\ nm}$) of 2.0×10^3 under 5 V bias when illuminated from back side. Combining theoretical analysis and experimental studies, it is demonstrated that the unique Ω-shaped structure plays a determined role in the performance enhancement. Additionally, this kind of Ω-shaped nanostructure could be migrated to other materials and served as a backbone in the next generation of electronics.

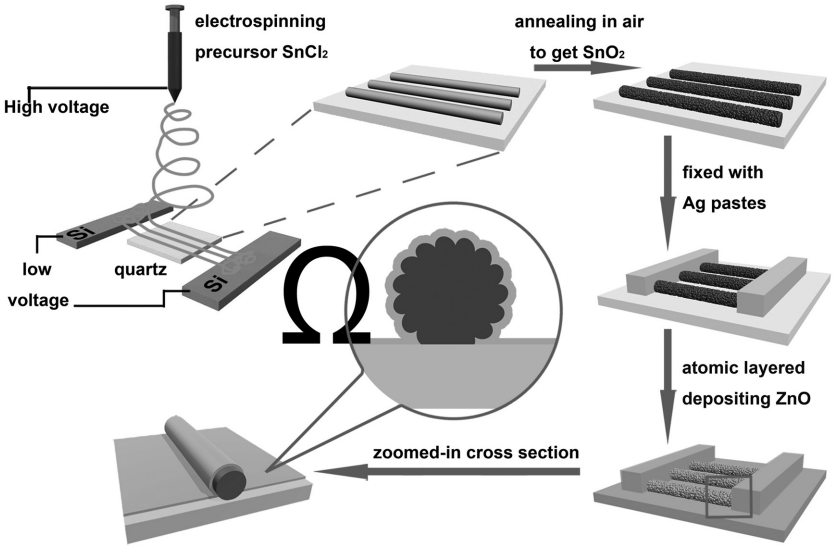

Scheme 1. Schematic diagram of the fabrication process.

2. Results

To fabricate an UV-selective enhanced PD, SnO_2 NFs arrays with Ω-shaped nanostructure ZnO layer have been constructed. As shown in **Scheme 1**, the preparation process includes two parts. First, SnO_2 NFs arrays on quartz were prepared using electric field-assisted electrospinning method,[23] followed by annealing at 550 °C for 3 h to remove organic parts (see the Experimental Section for details). After calcinations, a pair of silver electrodes with a sub-millimeter distance was pasted on the SnO_2 NFs to fix them and construct corresponding SnO_2-based PD. Second, a conformal Ω-shaped ZnO shell was coated on the obtained SnO_2 PD using ALD technique. On the merits of ALD, ZnO shell was deposited layer by layer with precise control of thickness. In our work, the number of ALD cycles was set as 100, equivalent to a thickness of 20 nm. The thickness of ZnO shell is comparable to its Debye length, benefit for enhancing the overall performance of device.[24]

Figure 1a,b shows the optical images of the as-prepared SnO_2 NF arrays with collecting time of 10 s and 10 min, respectively. The density of NFs is tuned by collecting time. Meanwhile, the orientation of arrays is determined by the assisting electric field applied on two collectors, where the electrostatic force pulls the liquid jet oppositely and guides the fibers onto the substrate.

We performed scanning electron microscopy (SEM) characterization to explore the morphology of SnO_2 NFs and SnO_2@ZnO

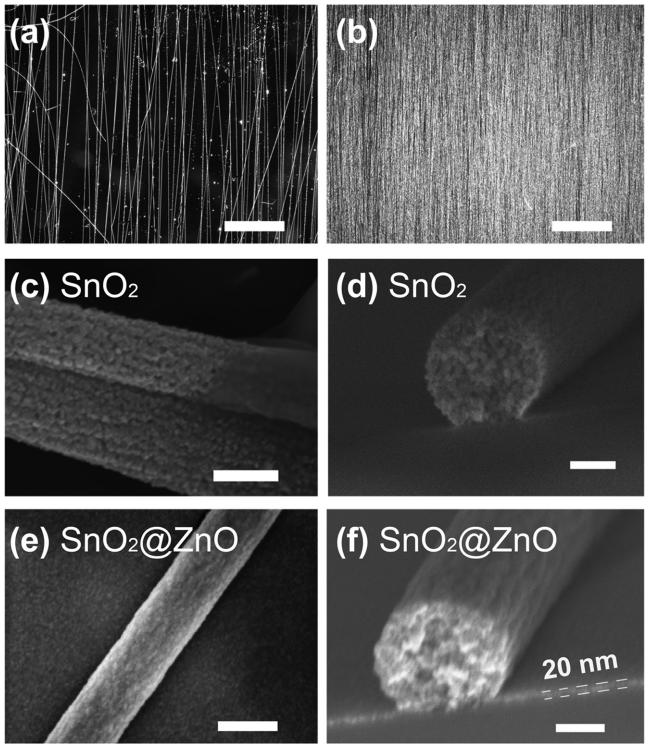

Figure 1. Optical microscopy images of ordered patterns with collecting time of a) 10 s and b) 10 min. c,e) plane-view and d,f) side view SEM images of SnO_2 NF and SnO_2@ZnO composite. Scale bars are 500 µm in (a) and (b), 200 nm in (c) and (e), and 100 nm in (d) and (f).

hybrid structure. Figure 1c shows SnO_2 NFs with an average diameter of ≈200 nm and a rough surface, which is a typical result of electrospinning.[25] Figure 1d shows the cross-section of the NF with a round shape and demonstrates a tight contact between SnO_2 NF and the substrate. These results reveal that the NFs are densely composed of enormous nanograins. After ALD process, the surface of the obtained SnO_2@ZnO composites becomes smooth, as shown in Figure 1e. The surface roughness of SnO_2 nanofibers and SnO_2@ZnO composites is measured as 24.2 and 16.9 nm with atomic force microscopy (results and more detailed discussion are shown in Figure S1, Supporting Information). Since the layer prepared by ALD method is compact and conformal,[26] the ZnO layer would fill the voids between SnO_2 nanograins, lowering surface roughness, which is in line with other reports.[27] The corresponding cross-section in Figure 1f reveals the Ω shape of SnO_2@ZnO hybrid structure. The thickness of ALD ZnO can be roughly estimated as 20 nm from the obtained layer on the adjacent substrate. Meanwhile, the outer shell covering the fiber should have similar thickness, except for the bottom of SnO_2 NFs. The thickness of ZnO was also further examined by ellipsometer on a ZnO-deposited silicon wafer after the same ALD deposition process.

Figure 2a shows the transmittance spectra of SnO_2@ZnO composite. It has ≈87.4% optical transmittance at 550 nm and more than 80% transparency in the visible range. As shown in the inset, a clear picture of Fudan University campus could be clearly seen through a piece of our sample (the color version of picture can be found in Figure S2, Supporting Information). Figure 2b shows the UV–vis absorbance spectra of SnO_2 NFs, ZnO film, and SnO_2@ZnO composite. It is worth noting that SnO_2@ZnO composite behaves as a summation of ZnO film and SnO_2 NFs. From 750 to 400 nm, all three samples exhibit weak absorbance. From 400 to 350 nm, the absorbance of ZnO dominates in that of SnO_2@ZnO composite, demonstrating a sharp absorption edge located at around 400 nm. From 350 to 280 nm, further increase in absorbance of SnO_2@ZnO composite might be caused by the absorbance of SnO_2, whereas ZnO film has no higher absorbance than its peak at 380 nm. From the absorbance diagram, the direct bandgap is determined as 3.8 eV for electrospun SnO_2 NFs and 3.2 eV for ALD ZnO film (as discussed in Figure S2, Supporting Information). In summary, SnO_2@ZnO composite can be predicted as a good candidate for UV detector due to its excellent selectivity in UV absorption.

The X-ray diffraction (XRD) was used to characterize the crystalline and phase of materials. After annealing, SnO_2 NF array was obtained and maintained the orientation feature. As shown in **Figure 3**a, all peaks can be designated to the tetragonal rutile phase of SnO_2 (JCPDS card No. 41–1445) without other noticeable impurity peaks. The sharp peaks confirm a highly crystalline structure obtained after calcination. The size of crystalline domains can be estimated by the Scherrer equation

$$D = K\lambda / \beta \cos\theta \quad (1)$$

where K is a shape factor set as unity, λ is the wavelength of X-ray, and β is the full width at half maximum of the intensity at Bragg angle θ. The size of crystalline domains D can be calculated as 12 nm from the highest peak at (110) facet. For SnO_2@ZnO composite, no significant peak of ZnO is observed, probably resulting from the thin layer of ZnO. The results are consistent with previous reports, which indicated the difficulty in picking out the peaks of ZnO via ALD less than 45 nm.[27]

We performed X-ray photoelectron spectroscopy (XPS) to verify the existence of ZnO in Figure 3b. XPS was conducted on the composite sample with a piece of Si substrate, using element C for calibration. The two symmetric peaks observed in Figure 3c correspond to Zn $2p_{3/2}$ and Zn $2p_{1/2}$ with spin–orbit splitting of 23.0 eV, verifying the normal state of Zn^{2+} in our sample.[28] Figure 3d displays the corresponding O 1s spectra fitted with three Gaussian peaks at 529.8, 531.3, and 532.6 eV for Zn—O bonds in the wurtzite structure of ZnO, H—O bonds in —OH group on its surface, and Si—O bonds on the surface of substrate Si, respectively.[29] The spectra of Zn and O confirm the existence of ZnO. The spectra in Sn 3d5 region indicate the existence of Sn (Figure S3, Supporting Information).

The optoelectronic properties of the obtained devices were carefully explored using Ag pastes as electrodes. For comparison, the corresponding SnO_2 NF-based PD was tested before ALD process. **Figure 4**a displays the *I–V* curves of PDs based on SnO_2 NFs and SnO_2@ZnO composite under dark condition and 280 nm UV illumination. Two PDs have a comparable dark current. The photocurrent of SnO_2 PD reaches ≈10 nA at 5 V, while SnO_2@ZnO PD shows an even higher photocurrent

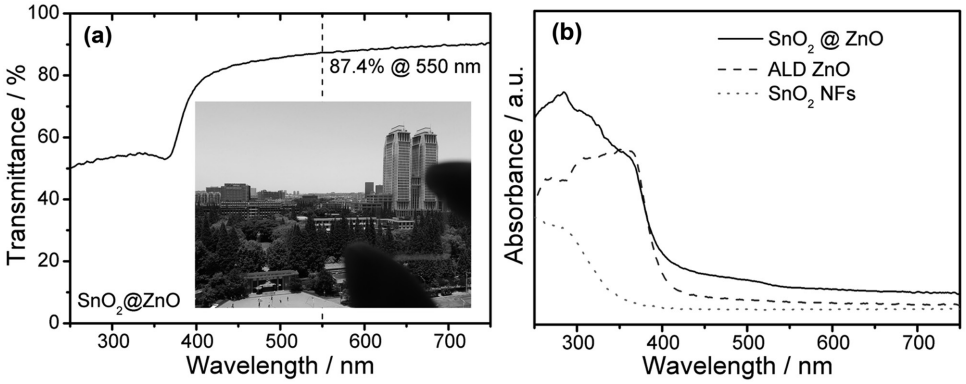

Figure 2. a) Transmittance of SnO_2@ZnO composite and the inset shows a picture of Fudan University campus (the colorful version can be found in the Supporting Information). b) UV–vis absorbance of SnO_2 NFs, ALD ZnO, and SnO_2@ZnO composite.

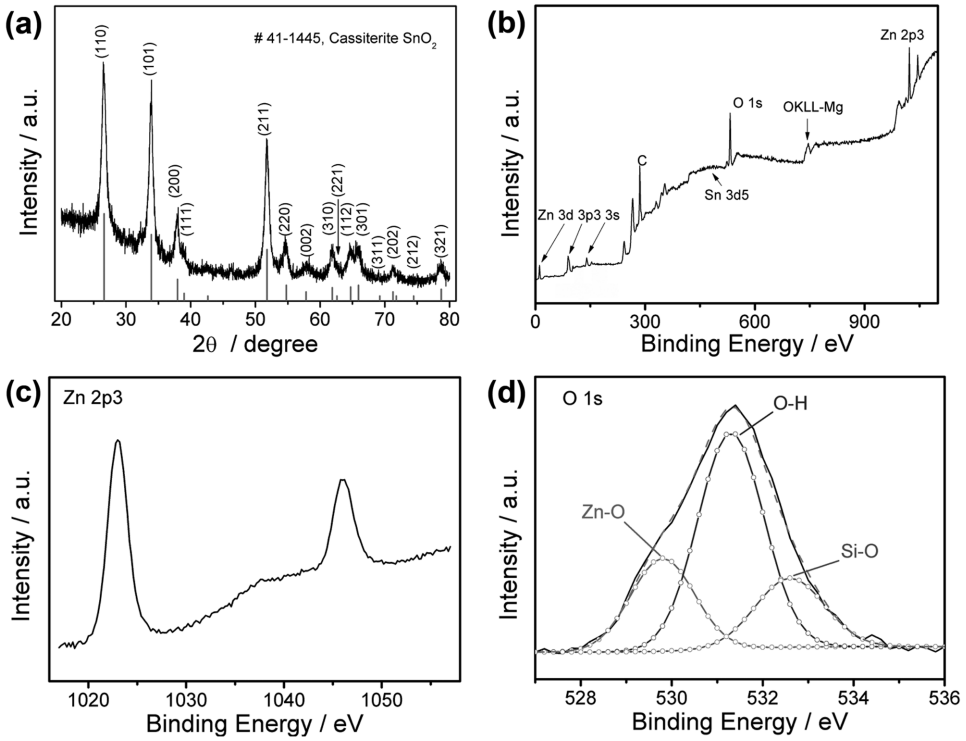

Figure 3. a) XRD patterns of SnO_2 NFs. b) Survey XPS spectra for SnO_2@ZnO hybrid structure and high resolution XPS spectra of c) Zn 2p3 and d) O 1s.

under the same condition, resulting in a photo-to-dark current ratio of 2×10^4. The linear and symmetric *I–V* curve of SnO_2 PD indicates good Ohmic contacts between SnO_2 and Ag pastes and verifies the structure as metal–semiconductor–metal (MSM) structure (Figure S4, Supporting Information). After depositing ZnO by ALD process, the linear property changes

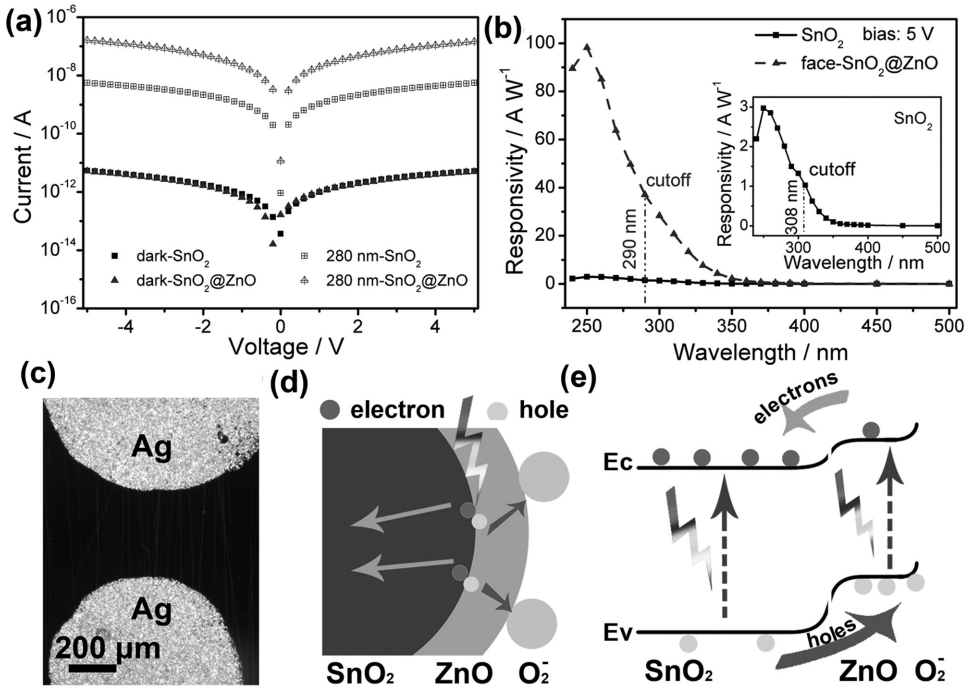

Figure 4. a) *I–V* curves of SnO_2 PD and SnO_2@ZnO PD illuminated with light of 280 nm wavelength and under dark. b) Responsivity spectra of SnO_2 PD and SnO_2@ZnO PD. c) Optical image of the corresponding device. d,e) Schematic diagrams of type-II energy band structure formed at the interface of SnO_2 and ZnO.

slightly, while the symmetry keeps maintaining the MSM structure. The optical photograph of the corresponding device is illustrated in Figure 4c.

The responsivity (R_λ) is a parameter to characterize the sensitivity of a PD, calculated by the equation

$$R_\lambda = \left(I_{ph} - I_d\right) / P_\lambda S \quad (2)$$

where I_{ph} and I_d are the photocurrent and dark current, P_λ is the light intensity at the wavelength λ, and S is the effective working area.[30] The spectral responsivity of SnO_2 PD and SnO_2@ZnO PD is calculated and plotted in Figure 4b. Here, we applied the same effective area of both PDs since adjacent ZnO film has a much less photoresponse compared to SnO_2 NFs (Figure S5, Supporting Information). SnO_2@ZnO PD displays a responsivity of ≈100 A W^{-1} under 5 V bias, which is 30-fold enhancement of SnO_2 PD (≈3 A W^{-1}). Compared to pure SnO_2 PD whose cutoff wavelength is 308 nm, SnO_2@ZnO PD has a shorter cutoff wavelength at 290 nm in UV range, both defined as the wavelength where the intensity is $1/e$ of the maximum intensity (e is nature constant ≈2.718).[12] Such an enhancement in photoresponse can be attributed to the modulated transportation behavior of photogenerated carriers at the interface.[31] Since electron affinities and bandgap energy levels of both materials are different, the band edge tends to bridge the offset at their boundary, forming a staggered type-II energy band structure and a built-in electric field. Under the UV illumination, photo-generated electron–hole pairs are separated by the built-in field. As shown in Figure 4d, driven by the field, holes tend to move into ZnO shell and electrons into SnO_2 core, reducing the probability of recombination.[32] Holes in the ZnO shell will be further attracted by absorbed O_2^- on the outer surface. Since the compact ZnO shell has a thickness of 20 nm, comparable to its Debye length,[24] nearly all photoinduced holes can enter the effective electric field range of O_2^-, reacting with O_2^-, and releasing the oxygen molecules. Electrons are able to diffuse fast inside SnO_2 NF with a high mobility.[19] The corresponding energy level diagram is shown in Figure 4e. When a bias voltage is applied at the two ends, the carriers will be extracted to electrodes in a short time.

In order to get more insight into the photoresponse of SnO_2@ZnO PD and explore the feature of Ω-shaped nanostructure, the wavelengths of UV light and the direction of incidence were varied, i.e., face illumination and back illumination. As indicated in Figure 2b, SnO_2 NFs absorb little at 350 nm while the other two have strong absorbance. Thus besides 280 nm, 350 nm light would be used as well in the following comparison. **Figure 5**a compares the dark current and photoresponse of SnO_2@ZnO PD to the light of 280 and 350 nm under face- and back-illumination conditions. These four response curves are all symmetric, verifying the MSM structure again. When illuminated from back side, SnO_2@ZnO PD has lower photoresponse to 350 nm light and higher photoresponse to 280 nm light, compared with that under face illumination. The highest photo-to-dark current ratio is 3.6×10^4, obtained under the condition of 280 nm light with back illumination. The linear I–V curves under 280 nm light are plotted in Figure 5b. The photocurrent obtained in back illumination increases almost twice compared with that in face illumination, especially from −1 to 1 V. And the curve obtained in back illumination shows a

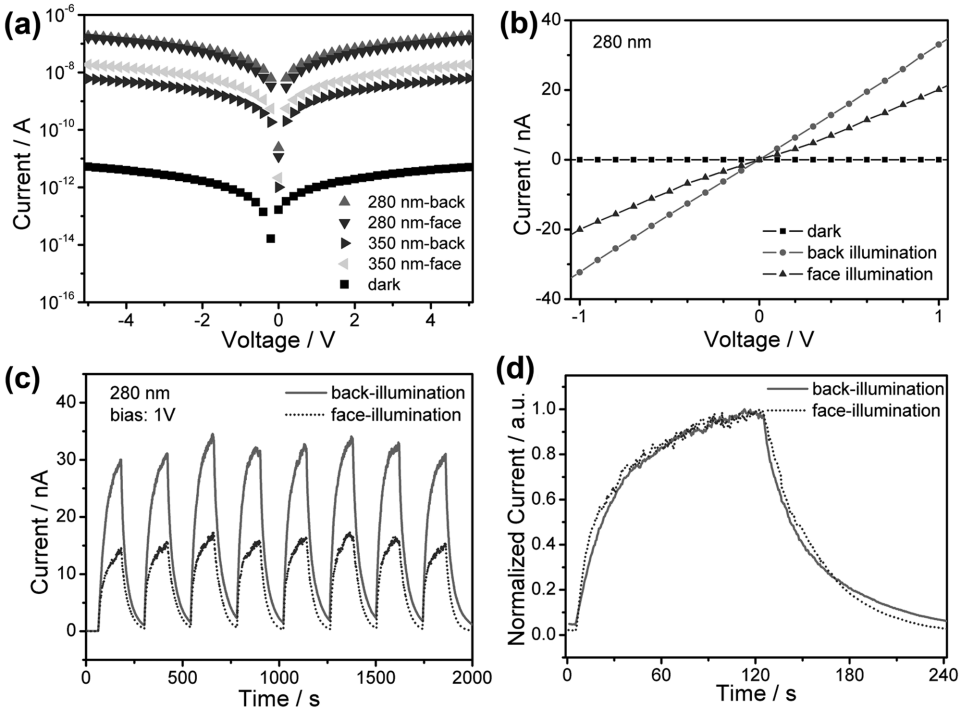

Figure 5. a) Logarithmic I–V curves of SnO_2@ZnO PD under dark and illuminated with a light of 280 or 350 nm in face- and back-illumination. b) Linear I–V curves of SnO_2@ZnO PD when back-illuminated by a light of 280 nm from −1 to 1 V. c) I–t curves of SnO_2@ZnO PD under a light of 280 nm at 1 V bias in face- and back-illumination. d) Comparison of normalized I–t curves in face- and back-illumination.

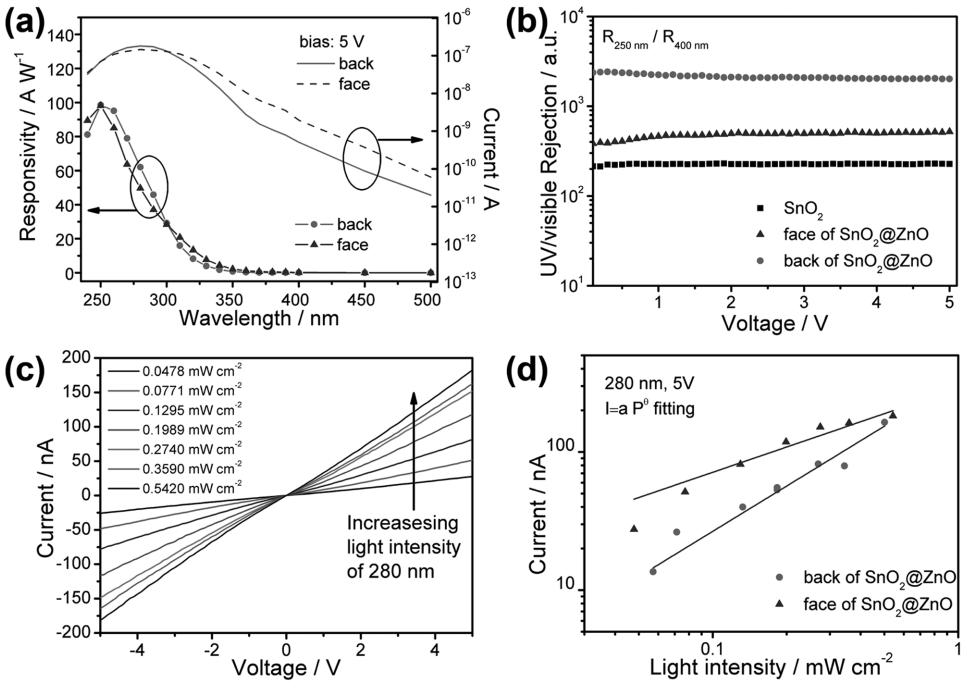

Figure 6. a) Responsivity and photocurrent spectra of SnO_2@ZnO PD at 5 V in face- and back-illumination. b) Plot of UV–vis rejection ratio ($R_{250\ nm}/R_{400\ nm}$) under various voltages. c) Light intensity-dependent *I–V* curves of SnO_2@ZnO PD under a light of 280 nm in back-illumination. d) Photocurrent of SnO_2@ZnO PD as a function of light intensity and corresponding fitting curves using the power law under 280 nm light in back- and face-illumination.

better linear property than in face one. The enhancement is also found in the time-dependent response, as depicted in Figure 5c. Among the eight cycles of on–off switching test with a bias of 1 V, the device shows stable photoresponse to 280 nm exposure. Back illumination gives a higher photocurrent around 30 nA while face one gives only 15 nA. Although the photocurrent increases, the trends of rise time and decay time remain the same under the two conditions, as revealed by current normalization curve in Figure 5d.

Figure 6a presents the spectroscopic responsivity of SnO_2@ZnO PD under the light of different wavelengths under back and face illumination. It is demonstrated that the responsivity increases as the wavelength decreases and the maximum is located at 250 nm which is ≈100 A W^{-1} under 5 V. However, the Ω-shaped structure differs the tendency of responsivity under back and face illumination. Under back illumination, the device gives a higher response below 300 nm, whereas a higher response is observed in face illumination from 500 to 300 nm. It means the back illumination can produce a higher UV selectivity, which is mathematically characterized as UV–vis rejection ratio. UV–vis rejection ratio is defined as the ratio between the highest responsivity in the UV region and the responsivity at 400 nm ($R_{250\ nm}/R_{400\ nm}$). In the semilog plot of responsivity (Figure S6, Supporting Information), UV–vis rejection ratios of different devices are compared. The SnO_2 PD itself possesses high UV selectivity with UV–vis rejection ratio of about 2.3×10^2, while SnO_2@ZnO hybrid PD under face illumination doubles it up to about 5.2×10^2. Furthermore, SnO_2@ZnO PD exhibits the highest value of 2.0×10^3 under 5 V and back illumination. It represents that the Ω-shaped structure produces an enhanced UV selectivity of the hybrid devices, especially under back illumination. In the Figure 6b, the rejection ratio ($R_{250\ nm}/R_{400\ nm}$) of different devices maintains its value under positive bias, showing a stable photoresponse. Besides, photo-to-dark current ratio at 280 nm is stable at positive bias (Figure S7, Supporting Information). Table S1 (Supporting Information) compares key parameters of photodetectors presented in this work and other relevant devices. As is well-known, the probability of photon-to-carrier generation is proportionally increased with increasing the absorbed photon flux. Figure 6c displays the linear *I–V* curves of SnO_2@ZnO PD under back illumination of 280 nm light with varying intensities, maintaining good linearity. Figure 6d plots the dependence of photocurrent of SnO_2@ZnO PD on the light intensity of 280 nm under both back and face illumination conditions with an applied voltage as 5 V. Each set of data can be fitted to a power law with different power indexes. The fitting of back illumination condition gives an index of 0.61 whereas it is 1.09 in the face illumination condition. It indicates that in the two cases, there are different processes of electron–hole generation, trapping, and recombination.[33]

The mechanism of the enhanced performance under back illumination is discussed from the viewpoint of optical field as well as photons. On the one hand, we performed finite-difference time domain (FDTD) simulations for the cross-section of SnO_2@ZnO, showing distributions of optical field around the nanostructure under face and back illumination. As shown in **Figure 7**a, 280 nm light coming from ZnO side is scattered by the air/ZnO interface and also leaks out through quartz, due to the dielectric mismatch in the refractive indexes of two materials.[34] Meanwhile, the intensity in the ZnO part is nearly zero

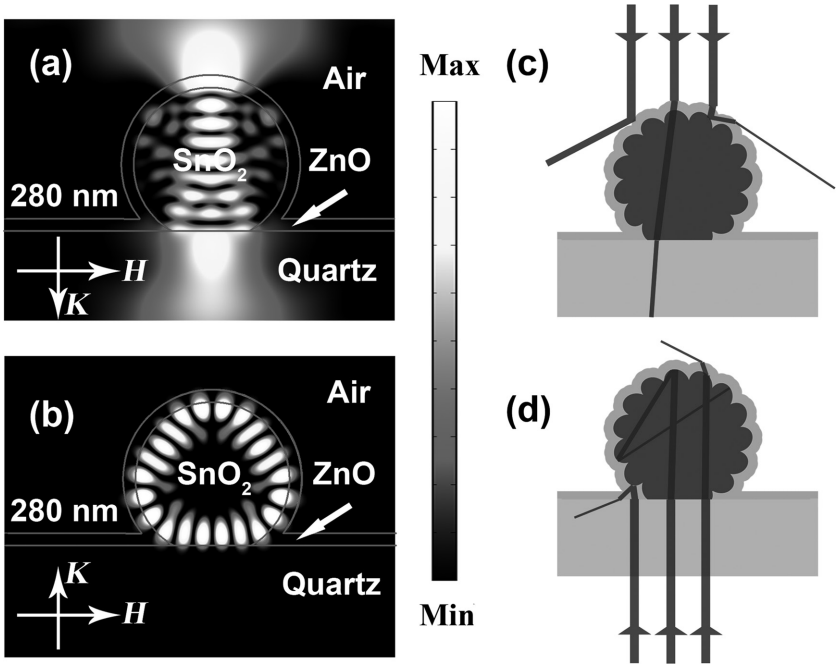

Figure 7. a,b) Theoretical simulations by FDTD method. c,d) Schematic diagrams of possible motion paths of incoming photons in face- and back-illumination configurations.

while in the nanofibers it is also weak and ambiguous, hindering the light usage. On the contrary, 280 nm light from quartz side is well confined inside the nanostructure by the outer shell with most intensity near the interface (Figure 7b), which sustains electromagnetic modes as whispering gallery mode.[35] It proves that the Ω-shaped structure is more effective to trap light coming from the back side. Once the light is trapped inside the structure, it will no doubt increase the probability of photon absorption. On the other hand, the shielding effect of ZnO layer might also contribute to the smaller current under face illumination. Figure 7c,d compares different possible photon paths of two conditions. Light coming from ZnO side should pass through ZnO first, and the effective number of photons absorbed by SnO_2 is less than that of original face-incident photons. However, when the light irradiates from the back side, SnO_2 can directly absorb photons and the existence of Ω-shaped ZnO layer prevents the unabsorbed photons from leaking out, in other words, confining them in the SnO_2 core. This shielding effect can be verified by transmittance spectra (Figure S8, Supporting Information), where the transmittance of ZnO in the UV range will be reduced by around 50% but that of SnO_2 is only 20%. In order to demonstrate the influence of Ω-shaped structure in this context, we constructed a comparative PD based on SnO_2@ZnO composite, where the ZnO layer was prepared by spin coating. As demonstrated in Figure S9 (Supporting Information), when back illuminated with 280 nm light, the photocurrent increases by two orders of magnitude, which is lower than our previous result. This difference might be attributed to that the ZnO layer covered on the SnO_2 nanofiber is uncompact (relevant SEM image is shown in Figure S10, Supporting Information), and thus the light might leak out from the cracks.[36] It is quite different from Ω-shaped structure, though the light comes from the SnO_2 side in both cases. Thus, from the perspective of both theoretical and experimental studies, it is safe to conclude that the modified photocurrent is mainly generated from the light trapping caused by our compact Ω-shaped structure.

3. Conclusion

In summary, an Ω-shaped SnO_2@ZnO hybrid UV photodetector is constructed after depositing ZnO layer on electrospun SnO_2 nanofiber arrays by ALD technique. This hybrid UV PD is transparent in visible range. It exhibits a high photo-to-dark current ratio of 3.6×10^4 at 280 nm and a high responsivity of $\approx 10^2$ A W^{-1} under 5 V at 250 nm light, which is 30 times higher than that of PD based on pristine electrospun SnO_2 nanofiber arrays. This enhancement is attributed to the type-II energy band structure at the ZnO/SnO_2 interface and the Ω-shaped nanostructure. With thorough investigation of SnO_2@ZnO PD under face- and back-illumination conditions, we have shown that the compact Ω-shaped structure plays a determined role in the photon gaining and trapping, as well as separating the electron–hole pair. The results reported in this paper would provide a facile route to fabricate low-dimensional UV photodetectors with high photocurrent. And the unique Ω-shaped nanostructure proposed in this work may open an additional opportunity for the future applications of optoelectronic devices.

4. Experimental Section

Fabrication of SnO_2 Nanofiber Arrays: Materials were all used as received without any purification. First, $SnCl_2{\cdot}2H_2O$ powder (0.6 g) was added into ethanol (2.5 mL) to obtain solution A. Meanwhile, solution B was a mixture of polyvinylpyrrolidone ($M \approx 1\,300\,000$ g mol^{-1}, 0.4 g) with *N*,*N*-dimethylformamide (2.3 mL) in water bath heated at 60 °C. After both solutions becoming clean and transparent, solution A was fast poured into solution B and the mixture was vigorously stirred for another 2 h. The final homogeneous precursor was colorless and then squeezed into the needle of a syringe at a feeding rate of 1.2 mL h^{-1}. Collectors were made of two pieces of silicon wafer without oxidized layer, which were parallel placed with 2 cm gap. A high voltage of 10 kV was applied at the tip of needle, and the collectors were connected with a negative voltage of –2 kV. The distance between collectors and the tip of needle was set around 20 cm. The electrospun NFs would form an array across the gap and they were manually fished up with a piece of quartz. The as-prepared organic NF arrays were then annealed in air at 550 °C for 3 h with the heating rate of 2 °C min^{-1}. The oxidized inorganic NF arrays on the quartz were obtained and a pair of Ag pastes was used as electrodes to construct the corresponding PD. The reason for the use of quartz is demonstrated from the view of transmittance spectra, as shown in Figure S11 (Supporting Information).

Fabrication of SnO_2@ZnO: After fixing the annealed NF arrays with two Ag pastes, a subsequent ALD was carried out in a chamber with deionized water and diethylzinc as vapor precursors. The gaseous elements were separately pumped as a pulse and reacted on the surface of substrate. A purge of nitrogen was introduced between two pulses to get rid of the residual. The temperature for reaction was kept at 200 °C

and the pressure was 1 Torr. Totally, 100 ALD cycles were performed in order to deposit a ZnO layer with 20 nm thickness.

Characterizations: The optical photographs of SnO_2 NFs were captured with a microscope. The morphologies of pure SnO_2 NFs and SnO_2@ZnO composite were characterized by field-emitting scanning electron microscope (Zeiss Sigma). The phases were identified by X-ray diffraction (Bruker D8-A25) using Cu Kα radiation (λ = 0.15406 nm) with 2θ ranging from 20° to 80°. The existence of ZnO was verified with X-ray photoelectron spectroscopy, which was carried out on a RBD 147 upgraded Perkin Elmer PHI 5000C ESCA system with Mg Kα (1253.6 eV) anode. Contaminant carbon (C 1s = 284.6 eV) was used to calibrate all the binding energies. The absorbance and transmittance spectra were recorded using UV–vis spectrophotometer (Hitachi U-3900H). The optoelectronic properties (*I–V* and *I–t* characteristics) were recorded with the semiconductor characterization system (Keithley 4200-SCS) in an environment with a temperature of 20 °C and humidity of 50%. A 75 W xenon arc lamp with a monochromator was used as light source.

Simulation: By means of the FDTD, optical field distribution and mode parameters of the Ω-shaped structure (SnO_2@ZnO) were theoretically calculated and simulated. The diameter of SnO_2 NFs was 250 nm while the thickness of ZnO layer was 20 nm. The refractive indexes of quartz, SnO_2, and ZnO were 1.5, 2.7, and 2.0, respectively.

Supporting Information

Supporting Information is available from the Wiley Online Library or from the author.

Acknowledgements

The authors would like to thank Dr. Longxing Su, Dr. Lingxia Zheng, and Mr. Weixin Ouyang for their help. This work was supported by the National Natural Science Foundation of China (Grant Nos. 11674061, 51471051, 61528402, 51372040, 61505033, 61376008), Science and Technology Commission of Shanghai Municipality (15520720700), MOST (No. 2016YFE0110700), Shanghai Rising-Star Program (16QA1400700), Shanghai Shu Guang Project (12SG01), and the Programs for Professor of Special Appointment (Eastern Scholar) at Shanghai Institutions of Higher Learning. Part of the experimental work has been carried out in Fudan Nanofabrication Laboratory.

Conflict of Interest

The authors declare no conflict of interest.

Keywords

Ω-shaped, atomic layer deposition, electrospinning, ultraviolet photodetectors, ultraviolet selectivity

Received: August 7, 2017
Revised: September 7, 2017
Published online: October 25, 2017

[1] a) D. I. Son, B. W. Kwon, D. H. Park, W. S. Seo, Y. Yi, B. Angadi, C.-L. Lee, W. K. Choi, *Nat. Nanotechnol.* **2012**, *7*, 465; b) M. Kim, C. Kwon, K. Eom, J. Kim, E. Cho, *Sci. Rep.* **2017**, *7*, 44411; c) Q. H. Wang, K. Kalantar-Zadeh, A. Kis, J. N. Coleman, M. S. Strano, *Nat. Nanotechnol.* **2012**, *7*, 699; d) N. Nasiri, R. Bo, T. F. Hung, V. A. L. Roy, L. Fu, A. Tricoli, *Adv. Funct. Mater.* **2016**, *26*, 7359.

[2] a) Z. L. Wang, *Mater. Sci. Eng., R* **2009**, *64*, 33; b) X. Pang, Y. He, J. Jung, Z. Lin, *Science* **2016**, *353*, 1268; c) X. Lu, C. Wang, Y. Wei, *Small* **2009**, *5*, 2349; d) R. Yan, D. Gargas, P. Yang, *Nat. Photonics* **2009**, *3*, 569.

[3] M. Willander, O. Nur, Q. X. Zhao, L. L. Yang, M. Lorenz, B. Q. Cao, J. Z. Pérez, C. Czekalla, G. Zimmermann, M. Grundmann, A. Bakin, A. Behrends, M. Al-Suleiman, A. El-Shaer, A. C. Mofor, B. Postels, A. Waag, N. Boukos, A. Travlos, H. S. Kwack, J. Guinard, D. L. S. Dang, *Nanotechnology* **2009**, *20*, 332001.

[4] H. Sun, Y. Zhang, J. Zhang, X. Sun, H. Peng, *Nat. Rev. Mater.* **2017**, *2*, 17023.

[5] M. Yu, Y. Z. Long, B. Sun, Z. Fan, *Nanoscale* **2012**, *4*, 2783.

[6] a) W. Tian, T. Zhai, C. Zhang, S. L. Li, X. Wang, F. Liu, D. Liu, X. Cai, K. Tsukagoshi, D. Golberg, Y. Bando, *Adv. Mater.* **2013**, *25*, 4625; b) X. Liu, L. L. Gu, Q. P. Zhang, J. Y. Wu, Y. Z. Long, Z. Y. Fan, *Nat. Commun.* **2014**, *5*, 4007. c) X. S. Fang, L. F. Hu, K. F. Huo, B. Gao, L. J.Zhao, M. Y. Liao, P. K. Chu, Y. Bando, D. Golberg, *Adv. Funct. Mater.* **2011**, *21*, 3907.

[7] a) L. Sang, M. Liao, M. Sumiya, *Sensors* **2013**, *13*, 10482; b) W. Tian, H. Lu, L. Li, *Nano Res.* **2015**, *8*, 382; c) T. Zhai, X. S. Fang, M. Liao, X. Xu, H. Zeng, B. Yoshio, D. Golberg, *Sensors* **2009**, *9*, 6504.

[8] a) H. Chen, H. Liu, Z. Zhang, K. Hu, X. S. Fang, *Adv. Mater.* **2016**, *28*, 403; b) Y. Xia, P. Yang, Y. Sun, Y. Wu, B. Mayers, B. Gates, Y. Yin, F. Kim, H. Yan, *Adv. Mater.* **2003**, *15*, 353.

[9] a) S. Xu, Z. L. Wang, *Nano Res.* **2011**, *4*, 1013; b) Q. Wei, F. Xiong, S. Tan, H. Lei, E. H. Lan, B. Dunn, L. Mai, *Adv. Mater.* **2017**, *29*, 1602300.

[10] a) M. Chen, L. Hu, J. Xu, M. Liao, L. Wu, X. S. Fang, *Small* **2011**, *7*, 2449; b) Z. Zheng, L. Gan, J. Zhang, F. Zhuge, T. Zhai, *Adv. Sci.* **2017**, *4*, 1600316; c) R. Viter, Z. Balevicius, A. Abou Chaaya, I. Baleviciute, S. Tumenas, L. Mikoliunaite, A. Ramanavicius, Z. Gertnere, A. Zalesska, V. Vataman, V. Smyntyna, D. Erts, P. Miele, M. Bechelany, *J. Mater. Chem. C* **2015**, *3*, 6815.

[11] H. Shi, B. Cheng, Q. Cai, X. Su, Y. Xiao, S. Lei, *J. Mater. Chem. C* **2016**, *4*, 8399.

[12] B. Zhao, F. Wang, H. Chen, L. Zheng, L. Su, D. Zhao, X. S. Fang, *Adv. Funct. Mater.* **2017**, *27*, 1700264.

[13] a) L. Hu, J. Yan, M. Liao, L. Wu, X. S. Fang, *Small* **2011**, *7*, 1012; b) C. Soci, A. Zhang, B. Xiang, S. A. Dayeh, D. P. Aplin, J. Park, X. Y. Bao, Y. H. Lo, D. Wang, *Nano Lett.* **2007**, *7*, 1003.

[14] L. Gan, M. Liao, H. Li, Y. Ma, T. Zhai, *J. Mater. Chem. C* **2015**, *3*, 8300.

[15] a) Z. He, Q. Liu, H. Hou, F. Gao, B. Tang, W. Yang, *ACS Appl. Mater. Interfaces* **2015**, *7*, 10878; b) K. Huang, Q. Zhang, F. Yang, D. He, *Nano Res.* **2010**, *3*, 281.

[16] a) L. Hu, J. Yan, M. Liao, H. Xiang, X. Gong, L. Zhang, X. S. Fang, *Adv. Mater.* **2012**, *24*, 2305; b) Z. Zheng, L. Gan, H. Li, Y. Ma, Y. Bando, D. Golberg, T. Zhai, *Adv. Funct. Mater.* **2015**, *25*, 5877.

[17] a) C. Y. Hsu, D. H. Lien, S. Y. Lu, C. Y. Chen, C. F. Kang, Y. L. Chueh, W. K. Hsu, J. H. He, *ACS Nano* **2012**, *6*, 6687; b) A. Kar, A. Patra, *J. Mater. Chem. C* **2014**, *2*, 6706.

[18] A. A. Chaaya, M. Bechelany, S. Balme, P. Miele, *J. Mater. Chem. A* **2014**, *2*, 20650.

[19] X. Li, C. Gao, H. Duan, B. Lu, Y. Wang, L. Chen, Z. Zhang, X. Pan, E. Xie, *Small* **2013**, *9*, 2005.

[20] S. Panigrahi, D. Basak, *Nanoscale* **2011**, *3*, 2336.

[21] P. N. Ni, C. X. Shan, S. P. Wang, X. Y. Liu, D. Z. Shen, *J. Mater. Chem. C* **2013**, *1*, 4445.

[22] F. Zhang, Y. Ding, Y. Zhang, X. Zhang, Z. L. Wang, *ACS Nano* **2012**, *6*, 9229.

[23] D. Li, Y. Wang, Y. Xia, *Nano Lett.* **2003**, *3*, 1167.

[24] S. W. Choi, A. Katoch, G. J. Sun, J. H. Kim, S. H. Kim, S. S. Kim, *ACS Appl. Mater. Interfaces* **2014**, *6*, 8281.

[25] Z. Zheng, L. Gan, T. Zhai, *Sci. China Mater.* **2016**, *59*, 200.
[26] F. Kayaci, C. Ozgitakgun, I. Donmez, N. Biyikli, T. Uyar, *ACS Appl. Mater. Interfaces* **2012**, *4*, 6185.
[27] S. W. Choi, J. Y. Park, S. S. Kim, *Nanotechnology* **2009**, *20*, 465603.
[28] Z. Zhang, C. Shao, X. Li, L. Zhang, H. Xue, C. Wang, Y. Liu, *J. Phys. Chem. C* **2010**, *114*, 7920.
[29] J. Yun, Y. Lim, H. Lee, G. Lee, H. Park, S. Y. Hong, S. W. Jin, Y. H. Lee, S. S. Lee, J. S. Ha, *Adv. Funct. Mater.* **2017**, *29*, 1700135.
[30] L. Zheng, K. Hu, F. Teng, X. S. Fang, *Small* **2017**, *13*, 1602448.
[31] A. Katoch, S. W. Choi, G. J. Sun, S. Kim, *J. Mater. Chem. A* **2013**, *1*, 13588.
[32] F. Teng, W. Ouyang, Y. Li, L. Zheng, X. S. Fang, *Small* **2017**, *13*, 1700156.
[33] H. Kind, H. Yan, B. Messer, M. Law, P. Yang, *Adv. Mater.* **2002**, *14*, 158.
[34] C. O. Aspetti, R. Agarwal, *J. Phys. Chem. Lett.* **2014**, *5*, 3768.
[35] C. H. Cho, C. O. Aspetti, J. Park, R. Agarwal, *Nat. Photonics* **2013**, *7*, 285.
[36] F. Teng, L. Zheng, K. Hu, H. Chen, Y. Li, Z. Zhang, X. S. Fang, *J. Mater. Chem. C* **2016**, *4*, 8416.